1 # Effective degradation of phenacetin in wastewater by

2 # (photo)electro-Fenton processes: Investigation of variables,

3 # acute toxicity, and intermediates

4 Ricardo Cardoso [a], Thalita Ferreira da Silva [a], Priscila Sabioni Cavalheri [a,b],

5 Beatriz Santos Machado [b], Carlos Eduardo Domingues Nazario [a], Amilcar

6 Machulek Junior [a], Ignasi Sirés [c,**], Fábio Gozzi [d], Silvio César de Oliveira

7 [a,*]

8 [a] *Institute of Chemistry, Federal University of Mato Grosso do Sul, Av, Senador Filinto*

9 *Muller, 1555, CEP 79074-460, Campo Grande - MS, Brazil*

10 [b] *Department of Sanitary and Environmental Engineering, Dom Bosco Catholic*

11 *University, Av, Tamandaré, 6000, CEP 79117-900, Campo Grande - MS, Brazil*

12 [c] *Laboratori d'Electroquímica dels Materials i del Medi Ambient, Departament de*

13 *Ciència de Materials i Química Física, Secció de Química Física, Facultat de Química,*

14 *Universitat de Barcelona, Martí i Franquès 1-11, 08028 Barcelona, Spain*

15 [d] *CMULTI-Multidisciplinary Center, Campus Floresta, Federal University of Acre,*

16 *Estrada da Canela Fina street, km 12, CEP 69895-000, Cruzeiro do Sul - AC, Brazil*

17

18

19 Submitted for publication in *Journal of Environmental Chemical Engineering*

20 * Corresponding author: silvio.oliveira@ufms.br (S. C. de Oliveira)

21 ** Corresponding author: i.sires@ub.edu (I. Sirés)

Abstract

Electro-Fenton (EF) and solar photoelectro-Fenton (SPEF) processes were employed at different scales to degrade phenacetin (PNT), the first synthetic analgesic. EF experiments were conducted at lab scale, whereas SPEF experiments were performed in an 8 L pre-pilot plant using an electrochemical filter-press cell. Under optimal conditions (25 mg L^{-1} PNT, 25.3 mg L^{-1} Fe^{2+}, and current density of 59.5 mA cm^{-2}), EF resulted in degradation and mineralization degrees of 83.9% and 45.2% at 14 and 230 min, respectively. Similarly, PNT was spiked into real wastewater from a municipal secondary treatment plant, resulting in degradation of 68.0% and mineralization of 39.4%, with an energy consumption of 7.0 kWh g^{-1}. The optimal conditions of SPEF (16.8 mg L^{-1} Fe^{2+} and current density of 45.9 mA cm^{-2}) led to degradation and mineralization degrees of 55.9% and 37.1% at 36 and 181 min, respectively, with a low energy consumption of 0.142 kWh g^{-1}. Both processes effectively detoxified the solutions, as demonstrated by tests with *Artemia salina* and *Lactuca sativa*. Three distinct degradation pathways were proposed based on the identification of eleven reaction intermediates formed upon •OH attack. In conclusion, the low energy cost of the SPEF process underscores its potential for pharmaceutical degradation in wastewater.

Keywords: Ecotoxicity; Electrochemical advanced oxidation process; Gas-diffusion electrode; Solar photoelectro-Fenton; Wastewater.

1. Introduction

The economic development associated with steep population growth, coupled with the increase in agricultural production, has occurred in parallel to the synthesis of numerous chemical compounds to raise welfare and life expectancy [1−3]. As a result, many of these compounds end up being released into wastewater through agricultural, industrial, urban, and recreational activities. This alters the water cycle, causing a direct impact on the environment [4]. Examples of these contaminants include agrochemicals [5], pharmaceuticals [6], aromatic hydrocarbons [7], and personal care products [8].

In recent decades, there has been a predominant focus on conventional pollutants, particularly the most toxic and persistent ones, regarding the impact of pollution from emerging contaminants. However, there has been a recent shift in attention towards pharmaceutical residues, which are considered pseudo-persistent due to their continuous release into water [9,10]. These compounds enter the environment through various pathways, notably via excretion, municipal and hospital waste disposal, and inadequate removal in wastewater treatment plants [10].

Phenacetin (PNT, N-(4-ethoxyphenyl)-acetamide) was the first synthetic analgesic, invented in 1887 to reduce fever [11]. Due to some strong side effects, its commercialization was banned in 1970 in several countries [12]. In 2012, PNT was classified as a Group 1 carcinogenic substance by the World Health Organization [13]. However, this drug is still permitted in medications, in combination with aminopyrine, aspirin, and aminophenazone [14,15], or is added illegally in illicit drugs such as cocaine and heroin [16]. PNT has been detected in wastewater at concentrations of up to 68.6 ng L^{-1} [17] and in surface water at 68.3 µg L^{-1} [18]. Due to its high solubility and toxicity, conventional water treatment techniques are not effective in removing PNT [19].

65 Therefore, the electrochemical advanced oxidation processes (EAOPs) seem an

66 interesting alternative to eliminate this type of pollutant [20,21].

67 The EAOPs belong to the broader group of AOPs, which are non-selective oxidation

68 methods based on the formation of reactive oxygen species. Among them, the hydroxyl

69 radical ($^{\bullet}OH$) is an extremely reactive and short-lived oxidant with a high standard redox

70 potential ($E^0 = 2.80$ V), capable of destroying most organic contaminants causing their

71 mineralization [22]. There exist different types of AOPs, such as ozonation [14],

72 conventional homogeneous Fenton [23] , UV/persulfate [24], heterogeneous Fenton [25],

73 and photo-Fenton [26,27]. The Fenton process was one of the first AOPs to be developed.

74 Its mechanism involves the decomposition of hydrogen peroxide in acidic medium

75 catalyzed by Fe^{2+} ions (Reaction (1)), yielding $^{\bullet}OH$ [28]. Despite its high effectiveness,

76 the Fenton process has some disadvantages such as the need for industrial H_2O_2, the

77 production of iron sludge, and excessive catalyst consumption [29,30].

78 $$H_2O_2 + Fe^{2+} + H^+ \rightarrow Fe^{3+} + H_2O + {}^{\bullet}OH \tag{1}$$
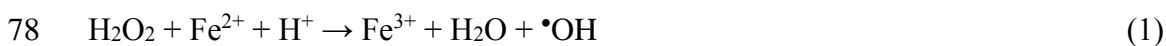
79 The electro-Fenton (EF) process has emerged to overcome these disadvantages [21]. EF

80 is based on the in-situ production of H_2O_2 from the two-electron reduction of O_2 (Reaction

81 (2) in an undivided electrochemical cell that contains an acidic solution with ferrous ions

82 [31,32]. UVA or sunlight irradiation can be incorporated to an EF system, resulting in the

83 corresponding UVA and solar photoelectro-Fenton (PEF and SPEF) processes [23,28,33].

84 $$O_2 + 2H^+ + 2e^- \rightarrow H_2O_2 \tag{2}$$
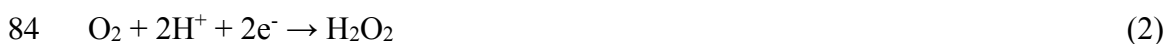
85 SPEF is a promising technology because clean and inexpensive sunlight is employed for

86 efficient catalysis. Solar photons enable the fast regeneration of Fe^{2+} ions, thereby

87   accelerating the production of $^{\bullet}OH$ from photoreduction Reaction (3). Furthermore, they

88   allow the photodecomposition of Fe(III) complexes via Reaction (4) [34,35].

89   $[Fe(OH)]^{2+} + h\nu \rightarrow Fe^{2+} + {}^{\bullet}OH$ \hfill (3)

90   $[Fe(OOCR)]^{2+} + h\nu \rightarrow Fe^{2+} + CO_2 + R^{\bullet}$ \hfill (4)
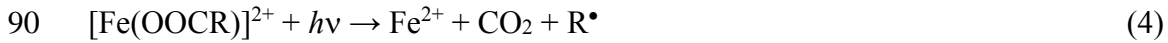
91   The catalytic Fe(III)/Fe(II) cycle shown in Reaction (1) is maintained while Fe^{2+} is

92   regenerated through Reactions (3) and (4), as well as through Fenton-like Reaction (5)

93   with hydrogen peroxide and by reaction with the hydroperoxyl radical ($HO_2^{\bullet}$) (Reaction

94   (6)) [21,36].

95   $Fe^{3+} + H_2O_2 \rightarrow Fe^{2+} + H^+ + {}^{\bullet}OH$ \hfill (5)

96   $Fe^{3+} + HO_2^{\bullet} \rightarrow Fe^{2+} + H^+ + O_2$ \hfill (6)

97   Although the use of the EAOPs has gained relevance in recent years for the treatment of

98   pharmaceuticals in water, most of the studies have been conducted on a laboratory scale

99   and using only model solutions. Few studies have assessed the oxidation power of this

100 technology for treating pharmaceuticals in real matrices on a larger scale [37].

101 In this work, the degradation and mineralization of PNT were first investigated by the EF

102 process at acidic pH in a stirred tank reactor. The experiments were conducted following

103 a central composite design (CCD) 2^4 factorial planning, aiming to optimize the treatment

104 by exploring the interactions between the independent variables: PNT and Fe^{2+}

105 concentrations, current density (j), and electrolysis time. The optimized laboratory

106 conditions were then applied to the treatment of real wastewater from a landfill by the

107 SPEF process in a pre-pilot unit. The main reaction intermediates accumulated during the

108 electrolysis were identified to elucidate the degradation pathways. Finally, the acute

109 toxicity of the treated solutions was tested using *Artemia salina* and *Lactuca sativa*.

2. Material and methods

2.1. Chemical reagents

Phenacetin (CAS No. 62-44-2, 98% purity), as well as catalase from bovine liver (2500

U mg^{-1}), were purchased from Sigma-Aldrich. Anhydrous sodium sulfate (99.5% purity),

ferrous sulfate heptahydrate (99.5% purity), sulfuric acid (98% purity), sodium hydroxide

(97% purity), ammonium metavanadate (99% purity), ferric nitrate (99.5% purity), *o*-

phenanthroline (99.5% purity), oxalic acid (99.5% purity), disodium hydrogen phosphate

(99% purity) and sodium dihydrogen phosphate (99% purity) were purchase from Vetec.

Acetonitrile of LC-MS grade was purchased from J.T. Baker. The other reagents used

were of HPLC or analytical grade. All samples were prepared using high-purity water

(resistivity > 18 MΩ cm at 25 ^{o}C) obtained from a Gehaka reverse osmosis water purifier

(model OS50 LX).

Real wastewater samples from the up-flow anaerobic sludge blanket (UASB) post-reactor

effluent (i.e., secondary effluent) were collected from a treatment plant in the municipality

of Campo Grande, Brazil (latitude 20°39'27.27" S; longitude 54°50'52.36" W). This plant

has an operational capacity of 1100 L s^{-1} and receives leachate produced by a public

landfill. The physicochemical characteristics of the effluent can be found in Table S1 (see

supplementary material).

2.2 Laboratory-scale EF and PEF experiments

The EF experiments were carried out in a jacketed electrochemical cell containing an air-

diffusion C/PTFE/C$_{cloth}$ (E-TEK, USA) cathode and a platinum plate (SEMPSA, Spain,

≥ 99%) as the anode, both with a geometric area of 3 cm^2 and placed at 1 cm from each

other. A 100 mL solution of PNT at specific concentrations and 0.05 mol L^{-1} Na$_2$SO$_4$ as

the electrolyte was employed for the electrolyses. The pH was adjusted to 3 with a 0.1

mol L^{-1} H$_2$SO$_4$ solution. The system was connected to a power supply (Instrutherm Fa-

135   3005), and all experiments were conducted at 25 °C by connecting the cell to a

136   recirculation water bath. The best experimental conditions found for the EF process were

137   applied to the PEF process for subsequent comparison with SPEF. For PEF, the same

138   system described for EF tests was employed, but adding a blacklight fluorescence lamp

139   (Philips TL/4W/08, λ_{max} = 360 nm, photon flux = 4.45 x 10^{21} photons s^{-1}) at about 6 cm

140   from the solution surface. In EF and PEF trials, the aliquots were collected at a given

141   electrolysis time.

142   A CCD 2^4 was applied to carry out the EF experiments. The factorial design involved four

143   independent variables: PNT concentration ([PNT], mg L^{-1}), Fe^{2+} concentration ([Fe^{2+}],

144   mg L^{-1}), current density (j, mA cm^{-2}), and time (min). The variables and their respective

145   levels are summarized in Table 1. Worth mentioning, the selected levels must comprise a

146   broad range of values for the variable under study, aiding to understand how independent

147   variables affect the dependent variable and to identify data patterns. Levels were chosen

148   based on prior studies, relevant literature, and existing theories. Preliminary experiments

149   were conducted to explore variable ranges and determine the most relevant levels for the

150   study. A total of 30 experiments were conducted, distributed as 16 cube points, 6 replicates

151   at the central point, and 8 axial points. All experimental designs in this work were

152   analyzed using the Minitab 19 statistical software program.

153

154   **Insert Table 1**

155

156   *2.3 SPEF experiments at pre-pilot scale*

157   The treatment of PNT by the SPEF process was carried out in a pre-pilot unit equipped

158   with an electrochemical filter-press-type cell, whose outlet was coupled to a planar solar

159   photoreactor (Figure S4, see Supplementary Material) [38]. The latter was a compound

160 parabolic collector (CPC) that comprised ten borosilicate glass tubes (internal diameter

161 of 28 mm, length of 851 mm, and thickness of 4 mm) connected in series by

162 polypropylene fittings, mounted on an aluminum platform tilted 15°. The experiments

163 were conducted on sunny days at the Institute of Chemistry, Federal University of Mato

164 Grosso do Sul, Brazil (latitude 20°30'20.6" S; longitude 54°37'02.1" W) [39]. The filter-

165 press-type reactor comprised a thin platinum plate as the anode and a C/PTFE air-

166 diffusion electrode (E-TEK, USA) as the cathode, both with an area of 20 cm^2. The back

167 surface of the cathode was faced with a gas chamber where a continuous air flow was

168 injected for H_2O_2 electrogeneration. In this study, each experiment was conducted with

169 an 8 L solution of 25 mg L^{-1} PNT previously dissolved in the effluent, whose pH was

170 adjusted to 3. The solution was constantly recirculated through the whole system by a

171 magnetic pump at a flow rate of 150 L h^{-1}. The electrochemical tests were conducted using

172 an Instrutherm Fa-3005 power supply. The UV radiation intensity was measured with a

173 luxmeter (AKSO AK-310) and subsequently converted to W m^{-2} [40] resulting in an

174 average value of 41.9 W m^{-2}.

175 A CCD 2^3 was applied to investigate and optimize the system variables. Three

176 independent variables were selected: initial catalyst concentration ([Fe^{2+}], mg L^{-1}), j (mA

177 cm^{-2}), and time (min). The corresponding levels for each variable are summarized in Table

178 1.

179 *2.4 Analytical procedures*

180 The PNT concentration in the experiments conducted in a model solution was chosen

181 using a previously described electrochemical treatment [14] The electrochemical

182 quantification of PNT was carried out in a conventional three-electrode cell. The working

183 electrode was a vitreous carbon electrode (geometric area of 1.10 cm^2), whereas Ag|AgCl

184 and Pt were employed as the reference and auxiliary electrodes, respectively. A 2.0-mL

185   sample of treated PNT solution was collected at different times, then added to 10.0 mL of

186   a 0.1 mol L^{-1} phosphate buffer solution, and finally introduced into the three-electrode

187   cell. The system was connected to an Autolab PGSTAT 302N potentiostat (Metrohm),

188   which was controlled by NOVA 2.1 software. Differential pulse voltammetry was

189   performed by setting the following parameters: potential increment, 0.004 V; pulse

190   amplitude, 0.05 V; pulse width, 0.05 s; sample width, 0.0167 s; pulse period, 0.2 s; and

191   quiet time, 2 s. The differential pulse voltammogram was recorded in the range of 0.4 to

192   1.2 V. Under these conditions, a calibration curve was constructed in the range of 0.0898

193   to 89.6000 mg L^{-1}, with a limit of detection (LOD) = 0.0583 mg L^{-1} and a limit of

194   quantification (LOQ) = 0.1750 mg L^{-1} (R^2 = 0.9990).

195   In the experiments conducted with real wastewater, the PNT concentration was

196   determined by high-performance liquid chromatography (HPLC) coupled with a UV/Vis

197   detector (Shimadzu SPD-M20A) set at 240 nm. Duplicate aliquots of 10 μL were injected

198   into a C18 column (Discovery$^{(R)}$ HS C18, dimensions 25 cm × 4.6 mm, 5 μm) from

199   Supelco Analytical, kept at 35 °C, using an isocratic method consisting of a mixture of

200   water acidified with 0.1% formic acid/acetonitrile (40:60 v/v), and the flow rate was set

201   at 0.8 mL min^{-1}. A calibration curve was obtained in the range of 0.0582 to 140 mg L^{-1},

202   with LOD = 0.0582 mg L^{-1} and LOQ = 0.1745 mg L^{-1} (R^2 = 0.9990). The concentration

203   values in mg L^{-1} of PNT, obtained either by voltammetry or HPLC, were converted to

204   degradation percentage using Equation (7):

205     $\%\text{Deg.} = \left(\frac{[PNT]_i - [PNT]_f}{[PNT]_f}\right) \times 100\%$ (7)

206   where [PNT]$_i$ and [PNT]$_f$ corresponds to the initial and final concentrations of PNT,

207   respectively.

208   The solution mineralization was monitored by measuring the total organic carbon analysis

209   (TOC) using the non-purgeable organic carbon analysis option of a Shimadzu TOC-V

210   analyzer. Before analysis, 2 mL aliquots were diluted in 5 mL of deionized water. The

211   results were obtained from a calibration curve with $LOQ = 0.180$ mg L^{-1} and $LOD = 0.053$

212   mg L^{-1}, and were converted to mineralization percentage according to Equation (8):

213    $\%Min. = \left(\frac{TOC_i - TOC_f}{TOC_f}\right) \times 100\%$ (8)

214   where TOC_i and TOC_f correspond to the initial and final values (in mg L^{-1}) of dissolved

215   organic carbon, respectively.

216   From the TOC analysis, it was possible to calculate the energy consumption per unit TOC

217   mass (EC_{TOC}, in kWh (g TOC)$^{-1}$)) using Equation (9) [41]:

218    $EC_{TOC} = \frac{E_{cell}\,It}{V_s \Delta(TOC)_{exp}}$ (9)

219   where E_{cell} is the average cell voltage (V), I is the applied current (A), t is the electrolysis

220   time (h), V_s is the volume of the treated solution (L), and $\Delta(TOC)_{exp}$ is the change in TOC

221   during the electrolysis (mg L^{-1}).

222   *2.5 By-products generation*

223   The identification of intermediates formed during the degradation of PNT was performed

224   by HPLC coupled with mass spectrometry (HPLC-MS). The system comprised a

225   Shimadzu LC-20AD chromatographic pump, a Kinetex-C18 column (2.6 μm, 150 mm ×

226   2.2 mm) kept at 50 °C, and a Bruker Daltonics MicrOTOF-QIII mass spectrometer with

227   an electron ionization source and a quadrupole time-of-flight detector operating in

228   positive and negative modes. The mobile phase was a water/acetonitrile mixture, each

229   containing 1% acetic acid, eluted according to a linear gradient at a flow rate of 0.3 mL

230   min^{-1}. The spectra were acquired in the *m/z* range of 120-600. The samples for HPLC-MS

231 analysis were obtained from the EF and SPEF treatments of PNT solutions at different

232 electrolysis times and j values.

233 *2.6 Acute toxicity analysis*

234 The acute toxicity tests were first conducted with *Artemia salina* nauplii, which was

235 incubated in a synthetic seawater solution (32 g L^{-1}) for 24 h under constant light

236 irradiation and aeration. The microcrustaceans were exposed to untreated and

237 electrochemically treated solutions, which were conditioned to the following dilution

238 concentrations: 70%, 50%, 25%, 12.5%, and 6.25% (v/v). A saline solution (32 g L^{-1}) was

239 used as the negative control, and a potassium dichromate solution (10 g L^{-1}) was used as

240 the positive control. The analysis was carried out at 25 ± 2 °C for 48 h, with a photoperiod

241 of 16 h of light and 8 h of darkness. Dead larvae were counted, and the median lethal

242 concentration (LC_{50}) was calculated using StatPlus AnalystSoft 8 software [31,42,43]. To

243 calculate the toxic units (TU), the equation TU = (1/LC_{50}) × 100 was used [44]. The

244 residual H_2O_2 should be removed from all samples before the analysis using a solution of

245 bovine catalase at 0.1 g L^{-1} [45].

246 The acute toxicity was also measured with *Lactuca sativa*. The bioassays were performed

247 in triplicate following a reported procedure [46]. For each assay, 15 commercial seeds

248 (ISLA) were placed in a germination paper inside a Petri dish, where 4 mL of the diluted

249 samples (70%, 50%, 25%, and 12,5%; v/v) were added, and the dishes were sealed and

250 stored in the dark for 120 h at 24 ºC [1]. Distilled water and 1% $Zn(NO_3)_2$ solution were

251 used as negative and positive controls, respectively. The residual H_2O_2 should be removed

252 from all samples before the analysis using a solution of bovine catalase at 0.1 g L^{-1} [45].

253 After 120 h, the size of the radicle of the germinated seeds was measured using a digital

254 caliper. The number of germinated seeds of the sample (GSS) and the radicle length of

255   the sample (RLS) were used to calculate the germination index (GI%), following

256   Equation (10).

257   $$GI\% = \frac{GSS \times RLS}{GSC \times RLC} \times 100 \qquad (10)$$

258   where GSC is the number of germinated seeds of the control and RLC, is the radicle

259   length of the control. The GI% values below 40% account for a significant inhibition,

260   between 40% and 80%, a slight inhibition, between 80% and 120%, no significant effect,

261   and above 120%, stimulation effect [47].

262   **3. Results and discussion**

263   *3.1 Factorial design for the EF process*

264   The CCD 2^4 was first used to investigate the PNT removal in a model solution. Table 2

265   summarizes the experimental and predicted degradation and mineralization responses for

266   each combination of variables under study.

267

268   **Insert Table 2**

269

270   The experimentally observed values and those predicted by the model exhibited a low

271   residual level, revealing a good fitting following the proposed methodology. Experiment

272   4 (highlighted in Table 2) showed the best performance, achieving a degradation of PNT

273   of 64.6% in 8 min and 35.2% mineralization in 130 min under the following operation

274   conditions: 25 mg L^{-1} [PNT], 29 mg L^{-1} [Fe^{2+}], and j = 60 mA cm^{-2}. On the other hand,

275   experiment 12 was the worse one, since it only exhibited 8.7% degradation in 5 min and

276   5.3% mineralization in 80 min, using 100 mg L^{-1} [PNT], 15 mg L^{-1} [Fe^{2+}], and j = 35 mA

277   cm^{-2}. These results demonstrate that the EF process is more effective at lower

278   concentrations of PNT and higher values of Fe^{2+}, j, and reaction time. When increasing

12

279   the value of these three parameters, the production of H_2O_2 and Fe^{2+} regeneration are

280   enhanced, leading to the generation of $^{\bullet}OH$ radicals that accelerate the contaminant

281   degradation. Conversely, at lower target compound concentrations, fewer amounts of

282   intermediates are produced, reducing their competition with PNT to react with $^{\bullet}OH$

283   radicals and hence, enhancing the process efficiency [48,49].

284   Table 3 presents the results of the analysis of variance (ANOVA) for the established model

285   regarding the degradation and mineralization data for PNT (results of Table 2). The model

286   suitability for PNT removal can be evaluated by analyzing the regression coefficients (R^2)

287   [50,51]. The degradation of PNT showed an R^2 value of 98.0%, while mineralization

288   showed 96.2%, leaving only 2.0% and 3.8% of the total variation unexplained by the

289   model. It is important to note that, despite the high significance of the model, the lack of

290   fit for PNT degradation was also statistically significant (p-value of 0.026 < 0.05). This

291   suggests that the model does not fully describe the relationship between the independent

292   variable and the response, possibly due to the exclusion of some important factor such as

293   interactions and quadratic terms. Furthermore, the lack of fit suggests the presence of

294   systematic variation not considered or explained by the statistical model. In the study, the

295   degradation performance of the [PNT] factor showed high significance in both the linear

296   term (p = 0.000, contribution of 49.3%) and the quadratic term (p = 0.000, contribution

297   of 10.5%), indicating variation not explained by the model.

298

299   **Insert Table 3**

300

301   All linear factors, quadratic terms [PNT]*[PNT], $[Fe^{2+}]*[Fe^{2+}]$, and *j*j*, and the

302   interaction $[Fe^{2+}]*j$ were statistically significant for PNT degradation. For mineralization,

303   all linear variables, quadratic terms $[Fe^{2+}]*[Fe^{2+}]$, *j*j*, and Time*Time, as well as the

304   interaction [PNT]*Time, were significant. Based on the results obtained, all evaluated

305   variables proved to be significant for the degradation of PNT.

306   Based on these results, the regression equations including only the significant factors for

307   degradation (Equation (11)) and mineralization (Equation (12)) were obtained,

308   evidencing the empirical relationship between the independent variables (X_i) and the

309   responses (Y_i) of the quadratic model.

310     $Y_{\%Deg.}$ = 15.1 − 1.305$X_{[PNT]}$ + 0.157$X_{[Fe^{2+}]}$ + 0.251X_j + 3.27X_{Time} +
311   0.00588($X_{[PNT]}*X_{[PNT]}$) − 0.00956($X_{[Fe^{2+}]}*X_{[Fe^{2+}]}$) − 0.0027($X_j*X_j$) + 0.0052($X_{[Fe^{2+}]}*X_j$)
312   (11)
313     $Y_{\%Min.}$ = -10.6 − 0.196$X_{[PNT]}$ + 0.299$X_{[Fe^{2+}]}$ + 0.371X_{Time} − 0.00466(X_j*X_j) −
314   0.00075($X_{Time}*X_{Time}$) − 0.00144($X_{[PNT]}*X_{Time}$)   (12)

315

316   *3.1.1 Degradation and mineralization of PNT by EF*

317   To evaluate the interaction effects of the independent variables and optimize the treatment

318   for PNT removal, three-dimensional surface plots were constructed based on the most

319   significant interactive effects inferred from the ANOVA results shown in Table 3. Since

320   the model involves more than two factors, two variables remain constant at the central

321   point while the other two vary within the experimental range.

322   Figure 1a presents the surface plot for PNT degradation constructed concerning the

323   variables [Fe^{2+}] and *j* while keeping constant [PNT] and time. The curvature in the graph

324   indicates higher efficiency at intermediate concentrations. This is because the quadratic

325   effect is highly significant and exerts a significant influence on the process. The increase

326   in current has a positive effect on the degradation of PNT since it leads to the production

327   of large quantities of H_2O_2, which enhances the reaction with ferrous ions and eventually

328   promotes the formation of $^{\bullet}OH$ [50]. However, very high currents tend to reduce the

329   efficiency of the process due to the occurrence of parasitic reactions, such as the formation

14

330 of H_2 at the cathode (Reaction (13)) and the partial scavenging of $^{\bullet}OH$ (Reaction (14))

331 [21,23]. A similar behavior was observed in other studies focused on the treatment of

332 pharmaceutical effluents by EF process [49,53].

333

334 $2H_2O + 2e^- \rightarrow H_{2(g)} + 2OH^-$ (13)

335 $H_2O_2 + {}^{\bullet}OH \rightarrow H_2O + HO_2{}^{\bullet}$ (14)

336

337 **Insert Figure 1**

338

339 In Figure 1b, the surface graph for PNT mineralization is plotted as a function of the

340 variables [PNT] and time, with $[Fe^{2+}]$ and j kept constant. The interaction between these

341 two variables is antagonistic because the efficiency of PNT removal significantly

342 increases at longer reaction times and lower PNT concentrations. This behavior agrees

343 with that reported by other authors [54].

344 By using the CCD 2^4 model, it was possible to obtain the optimal conditions for the

345 treatment of PNT. For maximizing the degradation and mineralization responses (Figure

346 S1, see supplementary material), the ideal conditions to treat PNT in the model solution

347 within the study range are as follows: 25 mg L^{-1} PNT, 25.3 mg L^{-1} Fe^{2+}, $j = 59.5$ mA cm$^-$

348 ^{2}, and reaction times of 14 min and 230 min for degradation and mineralization,

349 respectively. Under these optimized conditions, degradation and mineralization degrees

350 of 80.8% and 48.5%, respectively, are predicted. To confirm the theoretical operation

351 conditions suggested by computation, experiments were conducted in triplicate under

352 such conditions, yielding 83.9% ($\pm$ 1.6%) and 45.2% ($\pm$ 2.2%) removal for degradation

353 and mineralization, respectively. Therefore, it can be concluded that the developed model

15

354   is robust and highly predictive for the degradation and mineralization of PNT in a model

355   solution (i.e., Na_2SO_4 as the electrolyte) by EF process.

356   Once optimized the removal of PNT by EF process, the performance of this EAOP was

357   validated by treating PNT spiked into real wastewater produced in the secondary

358   treatment unit of a plant (Table 4). The obtained results showed 68.0% degradation and

359   39.4% mineralization of organic matter, with an energy consumption of 7.0 kW h (g

360   TOC)$^{-1}$. Although the EF process is highly efficient in degrading PNT, it encounters a

361   major issue such as the formation of iron(III) complexes ($[Fe(OOC-R)]^{2+}$, with Fe(III)-

362   carboxylate complexes as main example), which limit the reactivity. For this reason, the

363   method has been further improved by employing UVA radiation, leading to the PEF

364   process [28]. This method was also applied to the treatment of PNT in the real wastewater,

365   in triplicate, under the previously optimized conditions. Degradation and mineralization

366   of 89.5% and 68.7%, respectively, are observed under ideal operation conditions. The

367   results highlight a significant improvement in process effectiveness, particularly

368   regarding PNT mineralization. The results are listed in Table 4. The findings demonstrate

369   a significant improvement in PNT destruction. The application of UVA radiation favors

370   the regeneration of Fe^{2+} ions through the photoreduction of $[Fe(OH)]^{2+}$ (Reaction (3)) and

371   the photolysis of Fe(III) complexes (Reaction (4)), thereby promoting the generation of a

372   larger amount of hydroxyl radical [23].

373

374   **Insert Table 4**

375

376   *3.2 Factorial design for the SPEF process*

377   Based on the data obtained in section 3.1, the SPEF process was applied at pre-pilot scale

378   to treat the pollutant spiked into the real wastewater, maintaining the PNT concentration

379   at 25 mg L^{-1} and the solution pH at 3. For this system, a CCD 2^3 was adopted. Table 5

380   presents the experimental results obtained for the response factors (degradation and

381   mineralization percentages) and their respective predicted values. The observed values

382   are close to the predicted values, and the residuals are small, corroborating that the

383   proposed model is suitable.

384   The degradation analysis showed that experiment 16 (highlighted in Table 5) yielded the

385   best response, reaching 54.8% in 36 min, whereas experiment 7 led to 16.5% in 6 min,

386   under the same operational conditions. This suggests that the reaction time is the most

387   relevant variable for degrading PNT by SPEF process. Regarding mineralization,

388   experiment 3 (highlighted in Table 5) yielded the best result, with 33.9% at 150 min. On

389   the other hand, experiment 14 only reached 12.8% in 60 min, indicating that the TOC

390   abatement is highly dependent on all the independent factors (Fe^{2+}, j, and reaction time).

391

392   **Insert Table 5**

393

394   Table 6 displays the results of the ANOVA for the SPEF regression model. The model

395   correlation coefficients (R^2) and adjusted correlation coefficients (R^2_{Adj}) were developed

396   to predict the PNT degradation (R^2 = 98.5%; R^2_{Adj} = 96.6%) and mineralization (R^2 =

397   98.2%; R^2_{Adj} = 96.0%) degrees demonstrate a satisfactory fulfillment, with a high degree

398   of fitting. It is important to note that the contribution of the linear factor to the statistical

399   model is prevalent, accounting for 91.3% and 84.6% of the variance in degradation and

400   mineralization, respectively. In contrast, the quadratic and interaction terms were much

401   less relevant. For the degradation of PNT, all linear factors, the quadratic terms

402   [Fe^{2+}]*[Fe^{2+}] and Time*Time, and the interaction j*Time were statistically significant.

403 Regarding mineralization, all linear variables, the quadratic terms $j*j$ and Time*Time,

404 and the interactions $[Fe^{2+}]*j$ and $j*$Time were significant.

405

406 **Insert Table 6**

407

408 Thus, it was possible to obtain the equations of the developed model including just the

409 significant factors to predict the degradation and mineralization of PNT by SPEF process,

410 as shown in Equations (15) and (16).

411 $\mathbf{Y_{\%Deg.}} = -47.8 + 2.278X_{[Fe^{2+}]} + 0.919X_j + 2.915X_{Time} - 0.0546(X_{[Fe^{2+}]}*X_{[Fe^{2+}]}) -$
412 $0.01864(X_{Time}*X_{Time}) - 0.01944(X_j*X_{Time})$ (15)

413 $\mathbf{Y_{\%Min.}} = -21.03 + 2.001X_{[Fe^{2+}]} + 0.729X_j + 0.511X_{Time} - 0.0049(X_j*X_j) -$
414 $0.00127(X_{Time}*X_{Time}) - 0.02500(X_{[Fe^{2+}]}*X_j) + 0.011(X_j*X_{Time})$ (16)

415 *3.2.1 Degradation and mineralization of PNT by SPEF*

416 The effects of the operational parameters and their main interactions, as well as the

417 relationships between the independent variables and the response factors, are illustrated

418 using surface plots. Figure 2a, the mineralization plot is depicted in terms of $[Fe^{2+}]$ and j,

419 with time kept constant. The plot reveals a linear trend for Fe^{2+} content and a curvature

420 for j. This curvature is expected at high current values and can be associated with parasitic

421 reactions [21]. This suggests that the increase in the values of the variables must be limited

422 to avoid the recombination of $^{\bullet}OH$ caused by an excess of H_2O_2, which inhibits the

423 removal of PNT.

424

425 **Insert Figure 2**

426

18

427   Figures 2b and 2c present surface plots for the interaction between j and time, with $[Fe^{2+}]$

428   held constant. These variables show a synergistic effect, meaning that an increase in both

429   factors significantly improves the process efficiency.

430   The Minitab software was used to find the optimal conditions for the removal of PNT

431   from the secondary effluent using the SPEF process, which was as follows: $j = 45.9$ mA

432   cm^{-2}, $[Fe^{2+}] = 16.8$ mg L^{-1}, and reaction times of 36 min and 181 min for degradation and

433   mineralization, respectively (Figure S2, see supplementary material). Under these

434   conditions, the predicted values for PNT degradation and mineralization were 53.2% and

435   34.5%, respectively.

436   Trying to corroborate these results, experiments were conducted in triplicate using the

437   optimized conditions, and the results are presented in Table 7. As can be seen, 55.9%

438   degradation and 37.1% mineralization were achieved, with an energy consumption as low

439   as 0.142 kWh (g TOC)$^{-1}$. Note that the main reason for the limited mineralization degree

440   is likely the use of an active Pt anode. The Pt-$^{\bullet}$OH interaction is relatively strong and

441   hence, the radical has a great tendency to be converted to O_2 at the anodic surface,

442   resulting in a low oxidation power anode [55]. Additionally, some of the PNT by-products

443   may also hinder the mineralization [56]. Therefore, the statistical model applied to the

444   SPEF process proved to be effective and reliable in predicting the removal of PNT from

445   secondary effluent in a pre-pilot plant.

446

447   **Insert Table 7**

448

449   *3.3 PNT concentration decays and kinetic study*

450 The degradation profile of PNT was evaluated for EF and SPEF processes under the

451 optimized conditions. Figure 3 shows that the total degradation of PNT in ultrapure water

452 and real wastewater via EF occurred at 45 and 75 min, respectively. The SPEF treatment

453 in the actual wastewater using the much larger volume system (8 L solution) was slower,

454 requiring 120 min to complete PNT disappearance.

455

456   **Insert Figure 3**

457

458 The corresponding pseudo-first-order kinetic analysis [57] is shown in the inset of Figure

459 3, confirming the faster PNT removal in the order: EF (ultrapure water) > EF (effluent) >

460 SPEF (effluent, pilot unit).

461 The removal of PNT by EF in the model solution was particularly favored during the first

462 15 min of electrolysis, whereupon the reaction rate decreased significantly. As a result,

463 two distinct regions could be observed: a region with fast NT decay ($k = 0.317$ min^{-1}),

464 followed by a slower removal (not shown, $k = 0.108$ min^{-1}). In the first region, there is a

465 high availability of hydroxyl radicals, generated from the efficient decomposition of

466 hydrogen peroxide in the presence of Fe^{2+}. The appearance of the second region can be

467 associated with a reduced supply of ferrous ions and the accumulation of Fe(III)

468 complexes [46]. Byproducts formed during the degradation processes of PNT can

469 compete with the original organic compound for hydroxyl radical attack, reducing the

470 overall efficiency of degradation and resulting in the formation of persistent or

471 undesirable byproducts. Conversely, only one region is observed for the treatments in the

472 actual water matrix, with $k = 0.058$ and 0.027 min^{-1} by EF and SPEF processes,

473 respectively. The matrix complexity plays a very significant role, with several substances

474 acting as radical scavengers (i.e., inorganic ions, natural organic matter). Despite this, it

475   is worth noting that SPEF process is so powerful that it allows total PNT degradation in

476   120 min.

3.4 Acute toxicity

478   To evaluate this crucial aspect, the effect of the toxicity of the resultant solution after the

479   PNT treatment in the real wastewater was assessed using two different types of organisms,

480   *Artemia salina* and *Lactuca sativa*. To this purpose, samples collected from the effluents

481   treated by EF and SPEF processes under optimum mineralization conditions were

482   analyzed.

3.4.1 Toxicity to Artemia salina

484   The degradation of organic pollutants by AOPs has been widely reported in the literature.

485   However, despite their high effectiveness, they can often produce intermediates that are

486   more toxic than the original compound [43]. To evaluate this important aspect, the effect

487   of the toxicity of the by-products generated during the PNT treatment in the real

488   wastewater was assessed using larvae of the microcrustacean *Artemia salina*. The

489   organisms were employed to evaluate the toxicity of the model solution containing 25 mg

490   L^{-1} PNT, the raw secondary effluent, the solution containing 25 mg L^{-1} in the secondary

491   effluent, and the latter solution treated by EF and SPEF under optimized conditions. The

492   effectiveness of the EF and SPEF treatments to reduce toxicity is evidenced in Figure 4,

493   where the mortality rates are below 20%. As described by Persoone et al. [44], when TU

494   < 0.4, there is no acute toxicity; when 0.4 < TU < 1, there is slight acute toxicity; when 1

495   < TU < 10, there is acute toxicity; when 10 < TU < 100, there is high acute toxicity; and

496   TU > 100 indicates very high acute toxicity. The PNT solution in ultrapure water

497   exhibited slight acute toxicity, with a TU value of 0.7 ± 0.9. On the other hand, the real

498   effluent, both in the absence and presence of PNT, showed acute toxicity to *Artemia*

499   *salina*, with TU values of 1.4 ± 1.3 and 2.5 ± 1.2, respectively, indicating a water matrix

500 with high toxicity to the test organism [44]. Regarding the treated solutions, the sample

501 collected from the EF treatment at 230 min removed 89.6% of the toxicity, with a TU of

502 0.26 ± 1.4, indicating the absence of toxicity (TU < 0.4). Meanwhile, the toxicity of the

503 sample from the SPEF treatment at 181 min was reduced by 78.0%, with TU of $0.55 \pm$

504 0.06 that still denotes slight acute toxicity. The low efficacy in reducing toxicity is due to

505 the high sensitivity of the test organism and the low mineralization achieved (37.1%).

506

507 **Insert Figure 4**

508

509 *3.4.2 Toxicity to Lactuca sativa*

510 The toxic effect of the treated solutions on the germination rate of Lactuca sativa was

511 evaluated. Figure 5 shows the results of the *Lactuca sativa* germination index for the

512 different treatments. Before analysis, toxicity tests were carried out in various dilutions,

513 containing only Na_2SO_4 (0.05 mol L^{-1}), which did not show a significant difference in the

514 germination rate as compared to the control solution, with 94.5% similarity. For the raw

515 effluent, the effluent enriched with 25 mg L^{-1} of PNT, and the solution containing only 25

516 mg L^{-1} of PNT, no significant effects were found on seed germination, with GI% of

517 107.0%, 83.7% and 94.7%, respectively. This is consistent with previous studies that

518 showed no significant effects on germination after exposure to pharmaceuticals [58–60].

519 It is crucial to assess the toxicity of effluents treated by EF and SPEF, since the reaction

520 products formed may be more toxic than the original compounds. Concerning the

521 solutions treated under ideal mineralization conditions, the EF process showed no

522 toxicity, with a GI% of 82.3%. Meanwhile, the SPEF process showed little inhibition on

523 seed germination, with a GI% of 76.2%. This slight inhibition may be related to the

22

524   formation of toxic by-products formed upon oxidation of compounds present in the

525   effluent [61,62]. This means that mineralization degrees must be elevated to ensure high

526   detoxification.

527

528   **Insert Figure 5**

529

530   *3.5 Identification of intermediates and degradation routes for PNT*

531   The formation of reaction intermediates during the EF and SPEF treatments of PNT

532   solutions was studied by HPLC-MS. For this purpose, solutions containing 25 mg L^{-1}

533   PNT with 0.05 mol L^{-1} Na_2SO_4 at pH 3.0 were treated at different j values, and samples

534   were collected during the first 30 min of the experiment. Figure S3 (see supplementary

535   material) presents the mass spectra used to elucidate the potential degradation pathways,

536   which are illustrated in Figure 6. We propose three likely routes for the formation of

537   intermediates, corresponding to distinct hydroxylation sites on the PNT molecule.

538   In the first pathway (Route 1), the C-O bond of the benzene ring on PNT (**1**) is cleaved,

539   producing the hydroxylated compound *2* (*m/z* 151). This compound is identified as

540   acetaminophen, a well-known pharmaceutical [13], and a common metabolite of PNT

541   when administered to patients [63]. Although the cleavage of the N-C=O bond would

542   typically result in *p*-aminophenol (*m/z* 109), it was not detected in this case, likely due to

543   its transformation into compound **3** (*p*-nitrophenol) [64].

544   In the second pathway (Route 2), hydroxylated compound **4** (*m/z* 195) is generated

545   through the attack of the HO• on a free carbon site of the benzene ring [24], representing

546   the preferred route for the initial degradation of PNT [13]. The cleavage of the N-C=O

547   bond initiates a deacetylation reaction, yielding compound **5** (*m/z* 153) [65]. The amine

23

548   group undergoes oxidation to NO_2, resulting in compound **6** (*m/z* 183), which promptly

549   undergoes hydroxylate to produce compound **7** (*m/z* 199) [15]. Compound 7 undergoes

550   further oxidation caused by attack of the •OH resulting in compound **8** (m/z 197). (*m/z*

551   197). The subsequent opening of the aromatic ring leads to the formation of an aliphatic

552   carboxylic acid, compound **9** (*m/z* 231) [66]. In the third pathway (Route 3), the acetyl

553   group undergoes hydroxylation, forming compound **10** (*m/z* 195). It is noteworthy that

554   this is a secondary route for PNT degradation, as deacetylation is more favorable [67].

555   Subsequently, oxidation to the aldehyde occurs, yielding compound **11** (*m/z* 193),

556   followed by conversion to a carboxylic acid, compound **12** (*m/z* 181) [15].

557

558   **Insert Figure 6**

559

560   Table 8 summarizes the results achieved for PNT degradation in the present work via EF

561   and SPEF, as compared with those previously published by other methods [15,24,68–70].

562   As can be noted, a large removal can be attained within times of only 30 min, although

563   these are on a bench scale and in ultrapure water. The removal degrees found in our study

564   conducted at a pre-pilot scale suggest a promising direction for the application of SPEF

565   in actual wastewater.

566

567   **Insert Table 8**

568

569   **4. Conclusions**

570   The central composite design based on the response surface methodology adopted in this

571   work has served to optimize the experimental parameters for PNT oxidation through

572   EAOPs. The predicted results for PNT removal by EF and SPEF processes are in good

573   agreement with the experimental data. The SPEF unit with an 8 L capacity can treat PNT

24

574 in wastewater effluent, achieving 55.9% degradation in 36 min and 37.1% mineralization

575 in 181 min. Total PNT degradation is feasible in 120 min. The use of *Artemia salina* and

576 *Lactuca sativa* shows that EF and SPEF can detoxify the solutions sufficiently, needing a

577 slightly large electrolysis time in SPEF. Despite its high effectiveness efficiency, the

578 energy cost of the EF process is very high as compared to SPEF (7.0 vs 0.142 kWh (g

579 TOC)$^{-1}$). The latter is a very suitable method to treat a large volume of polluted

580 wastewater at low applied j.

588 **References**

589 [1] Da Silva, D. A., Cavalcante, R.P., Cunha, R.F., Machulek Jr., A., de Oliveira, S.C.,
590   2018. Optimization of nimesulide oxidation via a UV-ABC/H$_2$O$_2$ treatment
591   process: Degradation products, ecotoxicological effects, and their dependence on
592   the water matrix. Chemosphere 207, 457–468.
593   https://doi.org/10.1016/J.CHEMOSPHERE.2018.05.115.

594 [2] Li, Y., Wang, H., Deng, Y., Liang, D., Li, Y., Gu, Q., 2023. Applying water
595   environment capacity to assess the non-point source pollution risks in watersheds.
596   Water Res. 240, 120092. https://doi.org/10.1016/J.WATRES.2023.120092.

597 [3] Zhang, M., Sun, Q., Chen, P., Wei, X., Wang, B., 2022. How microorganisms tell
598   the truth of potentially toxic elements pollution in environment. J. Hazard. Mater.
599   431, 128456. https://doi.org/10.1016/J.JHAZMAT.2022.128456.

600 [4] El-Nahhal, I., El-Nahhal, Y., 2021. Pesticide residues in drinking water, their
601   potential risk to human health and removal options. J. Environ. Manage. 299,
602   113611. https://doi.org/10.1016/J.JENVMAN.2021.113611.

603 [5] Guelfi, D.R.V., Brillas, E., Gozzi, F., Machulek Jr., A., de Oliveira, S.C., Sirés, I.,
604   2019. Influence of electrolysis conditions on the treatment of herbicide bentazon
605   using artificial UVA radiation and sunlight. Identification of oxidation products. J.

606   Environ. Manage. 231, 213–221.
607   https://doi.org/10.1016/J.JENVMAN.2018.10.029.

608   [6]   Zhang, Y., Daniel, G., Lanzalaco, S., Isse, A.A., Facchin, A., Wang, A., Brillas, E.,
609   Durante, C., Sirés, I., 2022. H_2O_2 production at gas-diffusion cathodes made from
610   agarose-derived carbons with different textural properties for acebutolol
611   degradation in chloride media. J. Hazard. Mater. 423, 127005.
612   https://doi.org/10.1016/j.jhazmat.2021.127005

613   [7]   Luna, A.J., Chiavone-Filho, O., Machulek Jr, A., de Moraes, J.E.F., Nascimento,
614   C.A.O., 2012. Photo-Fenton oxidation of phenol and organochlorides (2,4-DCP
615   and 2,4-D) in aqueous alkaline medium with high chloride concentration. J.
616   Environ. Manage. 111, 10–17. https://doi.org/10.1016/J.JENVMAN.2012.06.014.

617   [8]   Zhou, C., Wang, Y., Tang, S., Wang, Y., Yu, H., Niu, J., 2021. Insights into the
618   electrochemical degradation of triclosan from human urine: Kinetics, mechanism
619   and toxicity. Chemosphere 264, 128598.
620   https://doi.org/10.1016/J.CHEMOSPHERE.2020.128598.

621   [9]   Ebele, A.J., Abdallah, M.A-E., Harrad, S., 2017. Pharmaceuticals and personal
622   care products (PPCPs) in the freshwater aquatic environment. Emerg. Contam. 3,
623   1–16. https://doi.org/10.1016/J.EMCON.2016.12.004.

624   [10]   Murrieta, M.F., Brillas, E., Nava, J.L., Sirés, I., 2023. Solar photoelectro-Fenton-
625   like process with anodically-generated HClO in a flow reactor: Norfloxacin as a
626   pollutant with a particular structure. Sep. Purif. Technol. 308, 122893.
627   https://doi.org/10.1016/J.SEPPUR.2022.122893.

628   [11]   Shibata, M.A, Sano, M., Hagiwara, A., Hasegawa, R., Shirai, T., 1995.
629   Modification by analgesics of lesion development in the urinary tract and various
630   other organs of rats pretreated with dihydroxy-di-N-propylnitrosamine and uracil.
631   Jpn. J. Cancer Res. 86, 160. https://doi.org/10.1111/J.1349-7006.1995.TB03034.

632   [12]   Daughton, C.G., Ruhoy, I.S., 2013. Lower-dose prescribing: Minimizing "side
633   effects" of pharmaceuticals on society and the environment. Sci. Total Environ.
634   443, 324–337. https://doi.org/10.1016/J.SCITOTENV.2012.10.092.

635   [13]   Li, W., Liu, B., Wang, Z., Wang, K., Lan, Y., Zhou, L., 2020. Efficient activation
636   of peroxydisulfate (PDS) by rice straw biochar modified by copper oxide (RSBC-
637   CuO) for the degradation of phenacetin (PNT). Chem. Eng. J. 395, 125094.
638   https://doi.org/10.1016/J.CEJ.2020.125094.

639   [14]   Yin, H., Meng, X., Xu, Z., Chen, L., Ai, S., 2012. Electrochemical behavior of
640   phenacetin on CdSe microspheres modified glassy carbon electrode and its
641   simultaneous determination with paracetamol and 4-aminophenol. Anal. Methods
642   4, 1445–1451. https://doi.org/10.1039/C2AY05912F.

643   [15]   Qi, F., Chu, W., Xu, B., 2015. Ozonation of phenacetin in associated with a
644   magnetic catalyst $CuFe_2O_4$: The reaction and transformation. Chem. Eng. J. 262,
645   552–562. https://doi.org/10.1016/J.CEJ.2014.09.068.

646   [16]   Broséus, J., Gentile, N., Bonadio Pont, F., Garcia Gongora, J.M., Gasté, L.,
647   Esseiva, P., 2015. Qualitative, quantitative and temporal study of cutting agents for
648   cocaine and heroin over 9 years. Forens. Sci. Int. 257, 307–313.
649   https://doi.org/10.1016/J.FORSCIINT.2015.09.014.

650   [17]   Mhuka, V., Dube, S., Nindi, M.M., 2020. Occurrence of pharmaceutical and
651   personal care products (PPCPs) in wastewater and receiving waters in South Africa

652   using LC-Orbitrap^{TM} MS. Emerg. Contam. 6, 250–258.
653   https://doi.org/10.1016/J.EMCON.2020.07.002.

654 [18] Gumbi, B.P., Moodley, B., Birungi, G., Ndungu, P.G., 2017. Detection and
655   quantification of acidic drug residues in South African surface water using gas
656   chromatography-mass spectrometry. Chemosphere 168, 1042–1050.
657   https://doi.org/10.1016/J.CHEMOSPHERE.2016.10.105.

658 [19] Bradley, P.M., Barber, L.B., Duris, J.W., Foreman, W.T., Furlong, E.T., Hubbard,
659   L.E., Hutchinson, K.J., Keefe, S.H., Kolpin, D.W., 2014. Riverbank filtration
660   potential of pharmaceuticals in a wastewater-impacted stream. Environ. Pollut.
661   193, 173–180. https://doi.org/10.1016/J.ENVPOL.2014.06.028.

662 [20] Gozzi, F., Sirés, I., de Oliveira, S.C., Machulek Jr., A., Brillas, E., 2018. Influence
663   of chelation on the Fenton-based electrochemical degradation of herbicide
664   tebuthiuron. Chemosphere 199, 709–717.
665   https://doi.org/10.1016/J.CHEMOSPHERE.2018.02.060.

666 [21] Martínez-Huitle, C.A., Rodrigo, M.A., Sirés, I., Scialdone, O., 2023. A critical
667   review on latest innovations and future challenges of electrochemical technology
668   for the abatement of organics in water. Appl. Catal. B: Environ. 328, 122430.
669   https://doi.org/10.1016/j.apcatb.2023.122430.

670 [22] Lanzalaco, S., Sirés, I., Galia, A., Sabatino, M.A., Dispenza, C., Scaildone, O.,
671   2018. Facile crosslinking of poly(vinylpyrrolidone) by electro-oxidation with IrO_2-
672   based anode under potentiostatic conditions. J. Appl. Electrochem. 48, 1343–1352.
673   https://doi.org/10.1007/s10800-018-1237-8.

674 [23] Oturan, M.A., Aaron, J.J., 2014. Advanced oxidation processes in
675   water/wastewater treatment: principles and applications. A review. Crit. Rev.
676   Environ. Sci. Technol. 44, 2577–2641.
677   https://doi.org/10.1080/10643389.2013.829765 44, 2577–2641.

678 [24] Gao, Y.-q., Zhou, J.-q., Zhang, J., Li, C., Gao, N.-y., Yin, D.-q., 2021. Factors
679   affecting UV/persulfate treatment of phenacetin and its disinfection by product
680   formation potential. Sep. Purif. Technol. 256, 117819.
681   https://doi.org/10.1016/J.SEPPUR.2020.117819.

682 [25] Ye, Z., Zhang, W., Lanzalaco, S., Zhao, L., Sirés, I., Xia, P., Zhai, J., He, Q., 2023.
683   Ultra-uniform $MIL-88B(Fe)/Fe_3S_4$ hybrids engineered by partial sulfidation to
684   boost catalysis in electro-Fenton treatment of micropollutants: Experimental and
685   mechanistic insights. Chem. Eng. J. 455, 140757.
686   https://doi.org/10.1016/j.cej.2022.140757.

687 [26] Cabrera-Reina, A., Miralles-Cuevas, S., Pérez, J.A.S., Salazar, R., 2021.
688   Application of solar photo-Fenton in raceway pond reactors: A review. Sci. Total
689   Environ. 800, 149653. https://doi.org/10.1016/j.scitotenv.2021.149653.

690 [27] Funai, D.H., Didier, F., Giménez, J., Esplugas, S., Marco, P., Machulek Jr., A.,
691   2017. Photo-Fenton treatment of valproate under UVC, UVA and simulated solar
692   radiation. J. Hazard. Mater. 323, 537–549.
693   https://doi.org/10.1016/J.JHAZMAT.2016.06.034.

694 [28] Cornejo, O.M., Sirés, I., Nava, J.L., 2023. Continuous H_2O_2 production sustained
695   by anodic O_2 for the destruction of the antibiotic ampicillin by photoelectro-Fenton
696   process in a rotating cylinder electrode reactor. J. Environ. Chem. Eng. 11, 109326.
697   https://doi.org/10.1016/j.jece.2023.109326.

698 [29] Friedrich, L.C., Mendes, M.A., Silva, V.O., Zanta, C.L.P.S., Machulek Jr., A.,
699 Quina, F.H., 2012. Mechanistic implications of zinc(II) ions on the degradation of
700 phenol by the fenton reaction. J. Braz. Chem. Soc. 23, 1372–1377.
701 https://doi.org/10.1590/S0103-50532012000700022.

702 [30] Droguett, C., Salazar, R., Brillas, E., Sirés, I., Carlesi, C., Marco, J.F., Thiam, A.,
703 2020. Treatment of antibiotic cephalexin by heterogeneous electrochemical
704 Fenton-based processes using chalcopyrite as sustainable catalyst. Sci. Total
705 Environ. 740, 140154. https://doi.org/10.1016/j.scitotenv.2020.140154.

706 [31] Da Silva, L.M.; Cavalcante, R.P.; Cunha, R.F.; Gozzi, F.; Dantas, R.F.; de Oliveira,
707 S.C.; Machulek Jr., A., 2016. Tolfenamic acid degradation by direct photolysis and
708 the UV-ABC/H_2O_2 process: factorial design, kinetics, identification of
709 intermediates, and toxicity evaluation. Sci. Total Environ. 573, 518–531.
710 https://doi.org/10.1016/J.SCITOTENV.2016.08.139.

711 [32] Guelfi, D.R.V., Gozzi, F., Machulek Jr., A., Sirés, I., Brillas, E., de Oliveira, S.C.,
712 2018. Degradation of herbicide S-metolachlor by electrochemical AOPs using a
713 boron-doped diamond anode. Catal. Today 313, 182–188.
714 https://doi.org/10.1016/J.CATTOD.2017.10.026.

715 [33] Zhang, Y., Daniel, G., Lanzalaco, S., Isse, A.A., Facchin, A., Wang, A., Brillas, E.,
716 Durante, C., Sirés, I., 2022. H_2O_2 production at gas-diffusion cathodes made from
717 agarose-derived carbons with different textural properties for acebutolol
718 degradation in chloride media. J. Hazard. Mater. 423, 127005.
719 https://doi.org/10.1016/j.jhazmat.2021.127005.

720 [34] Anotai, J., Singhadech, S., Su, C.C., Lu, M.C., 2011. Comparison of *o*-toluidine
721 degradation by Fenton, electro-Fenton and photoelectro-Fenton processes. J.
722 Hazard. Mater. 196, 395–401. https://doi.org/10.1016/J.JHAZMAT.2011.09.043.

723 [35] Guelfi, D.R.V., Ye, Z., Gozzi, F., de Oliveira, S.C., Machulek Jr., A., Brillas, E.,
724 Sirés, I., 2019. Ensuring the overall combustion of herbicide metribuzin by
725 electrochemical advanced oxidation processes. Study of operation variables,
726 kinetics and degradation routes. Sep. Purif. Technol. 211, 637–645.
727 https://doi.org/10.1016/J.SEPPUR.2018.10.029.

728 [36] Da Silva, L.M., Gozzi, F., Sirés, I., Brillas, E., de Oliveira, S.C., Machulek Jr., A.,
729 2018. Degradation of 4-aminoantipyrine by electro-oxidation with a boron-doped
730 diamond anode: Optimization by central composite design, oxidation products and
731 toxicity. Sci. Total Environ. 631–632, 1079–1088.
732 https://doi.org/10.1016/J.SCITOTENV.2018.03.092.

733 [37] Olvera-Vargas, H., Gore-Datar, N., Garcia-Rodriguez, O., Mutnuri, S., Lefebvre,
734 O., 2021. Electro-Fenton treatment of real pharmaceutical wastewater paired with
735 a BDD anode: Reaction mechanisms and respective contribution of homogeneous
736 and heterogeneous $^\bullet$OH, Chem. Eng. J. 404, 126524.
737 https://doi.org/10.1016/j.cej.2020.126524.

738 [38] Santos A.P.F., Gozzi, F., De Carvalho, A.E., De Oliveira, K.R.F., Caires, A.R.L.,
739 Cavalcante, R.P., Cunha, R.F., Da Silva, D.A, Guelfi, D.R.V., Da Silva, L.M., Da
740 Silva, T.F., Casagrande, G.A., De Oliveira, S.C., Machulek Jr, A., 2022. Leachate
741 degradation using solar photo-Fenton like process: Influence of coagulation-
742 flocculation as a pre-treatment step. Sep. Purif. Technol. 289, 120712.
743 https://doi.org/10.1016/J.SEPPUR.2022.120712.

744 [39] Dos Santos, P. R.; De Oliveira Dourados, M. E.; Sirés, I.; Brillas, E.; Cavalcante,
745   R. P.; Cavalheri, P. S.; Paulo, P. L.; Guelfi D. R. V.; Oliveira, C. S., Gozzi, F.,
746   Machulek Jr, A., 2023. Greywater treatment by anodic oxidation, photoelectro-
747   Fenton and solar photoelectro-Fenton processes: Influence of relevant parameters
748   and toxicity evolution. Process Safe. Environ. Protect. 169, 879-895.
749   https://doi.org/10.1016/j.psep.2022.11.058.
750 [40] Michael, P.R., Johnston, D.E., Moreno, W., 2020. A conversion guide: solar
751   irradiance and lux illuminance. J. Meas. Eng. 8, 153–166.
752   https://doi.org/10.21595/JME.2020.21667.
753 [41] Flox, C., Cabot, P.L., Centellas, F., Garrido, J.A., Rodríguez, R.M., Arias, C.,
754   Brillas, E., 2007. Solar photoelectro-Fenton degradation of cresols using a flow
755   reactor with a boron-doped diamond anode. Appl. Catal. B: Environ. 75, 17–28.
756   https://doi.org/10.1016/J.APCATB.2007.03.010.
757 [42] Cavalheri, P.S., Machado, B.S., Da Silva, T.F., de Oliveira, K.R.W., Magalhães
758   Filho, F.J.C., Nazário, C.E., Cavalcante, R.P., de Oliveira, S.C., Machulek Jr., A.,
759   2023. Ketoprofen and diclofenac removal and toxicity abatement in a real scale
760   sewage treatment Plant by photo-Fenton Process with design of experiments. J.
761   Environ. Chem. Eng. 11, 110699. https://doi.org/10.1016/J.JECE.2023.110699.
762 [43] Mesarič, T., Gambardella, C., Milivojević, T., Faimali, M., Drobne, D., Falugi, C.,
763   Makovec, D., Jemec, A., Sepčić, K., 2015. High surface adsorption properties of
764   carbon-based nanomaterials are responsible for mortality, swimming inhibition,
765   and biochemical responses in *Artemia salina* larvae. Aquat. Toxicol. 163, 121–129.
766   https://doi.org/10.1016/J.AQUATOX.2015.03.014.
767 [44] G. Persoone, B. Marsalek, I. Blinova, A. Törökne, D. Zarina, L. Manusadzianas,
768   G. Nalecz-Jawecki, L. Tofan, N. Stepanova, L. Tothova, B. Kolar, A practical and
769   user-friendly toxicity classification system with microbiotests for natural waters
770   and wastewaters, Environ Toxicol 18 (2003) 395–402.
771   https://doi.org/10.1002/tox.10141.
772 [45] Moreira, F.C., Soler, J., Fonseca, A., Saraiva, I., Boaventura, R.A.R., Brillas, E.,
773   Vilar, V.J.P., 2015. Incorporation of electrochemical advanced oxidation processes
774   in a multistage treatment system for sanitary landfill leachate. Water Res. 81, 375–
775   387. https://doi.org/10.1016/J.WATRES.2015.05.036
776 [46] Santos, D.H.S., Duarte, J.L.S., Tavares, M.G.R., Tavares, M.G., Friedrich, L.C.,
777   Meili, L., Pimentel, W.R.O., Tonholo, J., Zanta, C.L.P.S., 2020. Electrochemical
778   degradation and toxicity evaluation of reactive dyes mixture and real textile
779   effluent over DSA® electrodes. Chem. Eng. Process. Process Intensif. 153, 107940.
780   https://doi.org/10.1016/J.CEP.2020.107940.
781 [47] Cesaro, A., Belgiorno, V., Guida, M., 2015. Compost from organic solid waste:
782   Quality assessment and European regulations for its sustainable use. Res. Cons.
783   Rec. 94, 72-79. https://doi.org/10.1016/j.resconrec.2014.11.003.
784 [48] Bravo-Yumi, N., Pacheco-Álvarez, M., Bandala, E.R., Brillas, E., Peralta-
785   Hernández, J.M., 2022. Studying the influence of different parameters on the
786   electrochemical oxidation of tannery dyes using a Ti/IrO$_2$-SnO$_2$-Sb$_2$O$_5$ anode.
787   Chem. Eng. Process. Process Intensif. 181, 109173.
788   https://doi.org/10.1016/j.cep.2022.109173.
789 [49] Jin, Y., Huang, P., Chen, X., Li, L.P., Lin, C.Y., Chen, X., Ding, R., Liu, J., Chen,
790   R., 2023. Ciprofloxacin degradation performances and mechanisms by the

791 heterogeneous electro-Fenton with flocculated fermentation biochar. Environ
792 Pollut. 324, 121425. https://doi.org/10.1016/j.envpol.2023.121425.

793 [50] Asadollahzadeh, M., Tavakoli, H., Torab-Mostaedi, M., Hosseini, G., Hemmati,
794 A., 2014. Response surface methodology based on central composite design as a
795 chemometric tool for optimization of dispersive-solidification liquid–liquid
796 microextraction for speciation of inorganic arsenic in environmental water
797 samples. Talanta 123, 25–31. https://doi.org/10.1016/J.TALANTA.2013.11.071.

798 [51] Chaker, H., Attar, A.E., Djennas, M., Fourmentin, S., 2021. A statistical modeling-
799 optimization approach for efficiency photocatalytic degradation of textile azo dye
800 using cerium-doped mesoporous ZnO: A central composite design in response
801 surface methodology. Chem. Eng. Res. Design 171, 198–212.
802 https://doi.org/10.1016/J.CHERD.2021.05.00.

803 [52] Ghjair, A.Y., Abbar, A.H., 2023. Applications of advanced oxidation processes
804 (Electro-Fenton and sono-electro-Fenton) for COD removal from hospital
805 wastewater: Optimization using response surface methodology. Process Safe.
806 Environ. Protect. 169, 481–492. https://doi.org/10.1016/J.PSEP.2022.11.039.

807 [53] Jiménez-Bambague, E.M., Madera-Parra, C.A., Rangel-Delgado, M.F., Quintero-
808 Martinez, I., Miranda-Mosquera, D., Aristizabal-Apolinar, J.S., Machuca-
809 Martínez, F., 2023. Photo-Fenton and Electro-Fenton performance for the removal
810 of pharmaceutical compounds in real urban wastewater. Electrochim. Acta 442,
811 141905. https://doi.org/10.1016/J.ELECTACTA.2023.141905.

812 [54] Nasr Esfahani, K., Farhadian, M., Solaimany Nazar, A.R., 2019. Interaction effects
813 of various reaction parameters on the treatment of sulfidic spent caustic through
814 electro-photo-Fenton. Int. J. Environ. Sci. Technol. 16, 7165–7174.
815 https://doi.org/10.1007/s13762-018-2126-8.

816 [55] Kapałka, A., Fóti, G., Comninellis, C., 2007. Kinetic modelling of the
817 electrochemical mineralization of organic pollutants for wastewater treatment. J.
818 Appl. Electrochem. 38, 7–16. https://doi.org/10.1007/s10800-007-9365-6.

819 [56] Wu, J., Wang, B., Cagnetta, G., Huang, J., Wang, Y., Deng, S., Yu, G., 2020.
820 Nanoscale zero valent iron-activated persulfate coupled with Fenton oxidation
821 process for typical pharmaceuticals and personal care products degradation. Sep.
822 Purif. Technol. 239, 116534. https://doi.org/10.1016/j.seppur.2020.116534.

823 [57] Da Silva, T.F., Cavalcante, R.P., Guelfi, D.R.V., de Oliveira, S.C., Casagrande,
824 G.A., Caires, A.R.L., de Oliveira, F.F., Gubiani, J.R., Cardoso, J.C., Machulek Jr.,
825 A., 2022. Photo-anodes based on B-doped TiO_2 for photoelectrocatalytic
826 degradation of propyphenazone: Identification of intermediates, and acute toxicity
827 evaluation. J. Environ. Chem. Eng. 10, 107212.
828 https://doi.org/10.1016/J.JECE.2022.107212.

829 [58] Hillis, D.G., Flecher, J., Solomon, K.R.; Sibley, P.K., 2011. Effects of ten
830 antibiotics on seed germination and root elongation in three plant species. Arch.
831 Environ. Cont. Toxicol., 60, 220-232. https://doi.org/10.1007/s00244-010-9624-0.

832 [59] Pino, M.R., Muñiz, S., Val, J., Navarro, E., 2016. Phytotoxicity of 15 common
833 pharmaceuticals on the germination of Lactuca sativa and photosynthesis of
834 Chlamydomonas reinhardtii. Environ. Sci. Pollut. Res. 23, 22530-22541.
835 https://doi.org/10.1007/s11356-016-7446-y.

836 [60] Rede, D., Santos, L. H., Ramos, S., Oliva-Teles, F., Antão, C., Sousa, S. R.,
837 Delerue-Matos, C., 2019. Individual and mixture toxicity evaluation of three

838　　　pharmaceuticals to the germination and growth of Lactuca sativa seeds. Sci. Total.
839　　　Env. 673, 102-109. https://doi.org/10.1016/j.scitotenv.2019.03.432.

840　[61]　Martínez-Pachón, D., Botero-Coy, A. M., Hernandez, F., López, N. L., Torres-
841　　　Palma, R. A., Moncayo-Lasso, A., 2022. Elimination of contaminants of emerging
842　　　concern and their environmental risk in world-real municipal wastewaters by
843　　　electrochemical advanced oxidation processes. J. Environ. Chem. Eng. 10, 107803.
844　　　https://doi.org/10.1016/j.jece.2022.107803.

845　[62]　Montañés, M.T., García-Gabaldón, M., Roca-Pérez, L., Giner-Sanz, J.J., Mora-
846　　　Gómez, J., Pérez-Herranz, V., 2020. Analysis of norfloxacin ecotoxicity and the
847　　　relation with its degradation by means of electrochemical oxidation using different
848　　　anodes.　　Ecot.　　Environ.　　Safe.　　188,　　109923.
849　　　https://doi.org/10.1016/j.ecoenv.2019.109923.

850　[63]　Xiao, M., Zhang, Y., 2016. Electro-catalytic oxidation of phenacetin with a three-
851　　　dimensional reactor: Degradation pathway and removal mechanism. Chemosphere
852　　　152, 17–22. https://doi.org/10.1016/J.CHEMOSPHERE.2015.12.026.

853　[64]　Moctezuma, E., Leyva, E., Aguilar, C.A., Luna, R.A., Montalvo, C., 2012.
854　　　Photocatalytic degradation of paracetamol: Intermediates and total reaction
855　　　mechanism.　　J.　　Hazard.　　Mater.　　243,　　130–138.
856　　　https://doi.org/10.1016/J.JHAZMAT.2012.10.010.

857　[65]　Canle L., M., Santaballa, J.A., Vulliet, E., 2005. On the mechanism of TiO_2-
858　　　photocatalyzed degradation of aniline derivatives. J. Photochem. Photobiol. A
859　　　Chem. 175, 192–200. https://doi.org/10.1016/J.JPHOTOCHEM.2005.05.001.

860　[66]　Qi, F., Chu, W., Xu, B., 2016. Comparison of phenacetin degradation in aqueous
861　　　solutions by catalytic ozonation with $CuFe_2O_4$ and its precursor: Surface
862　　　properties, intermediates and reaction mechanisms. Chem. Eng. J. 284, 28–36.
863　　　https://doi.org/10.1016/J.CEJ.2015.07.095.

864　[67]　Yun, C.H., Miller, G.P., Guengerich, F.P., 2000. Rate-determining steps in
865　　　phenacetin oxidations by human cytochrome P450 1A2 and selected mutants.
866　　　Biochemistry 39, 11319–11329. https://doi.org/10.1021/BI000869U.

867　[68]　Tan, C., Sheng, T., Xu, Q., Xu, T., Sun, K., Deng, L., Xu, W., 2021. Cobalt doped
868　　　iron oxychloride as efficient heterogeneous Fenton catalyst for degradation of
869　　　paracetamol　　and　　phenacetin.　　Chemosphere　　263,　　127989.
870　　　https://doi.org/10.1016/j.chemosphere.2020.127989.

871　[69]　Gao, Y., Rao, Y., Ning, H., Yin, D., Gao, N., 2021. MoS_2-assisted
872　　　Fe^{2+}/peroxymonosulfate oxidation for the abatement of phenacetin: efficiency,
873　　　mechanisms　and　toxicity　evaluation.　RSC　Adv　11,　33149–33159.
874　　　https://doi.org/10.1039/d1ra05892d.

875　[70]　Zhu, Y., Wu, M., Gao, N., Chu, W., Li, K., Chen, S., 2018. Degradation of
876　　　phenacetin by the UV/chlorine advanced oxidation process: Kinetics, pathways,
877　　　and　　toxicity　　evaluation.　　Chem.　　Eng.　　J.　　335,　　520–529.
878　　　https://doi.org/10.1016/j.cej.2017.10.070.

879

Figure captions

Figure 1. Surface plots illustrate the interaction between (a) $[Fe^{2+}]$ and current density for PNT degradation, and between (b) [PNT] and reaction time for PNT mineralization by EF process in a model solution.

Figure 2. Surface plots illustrate the interaction between factors: (a) $[Fe^{2+}]$ and j for PNT mineralization, as well as j and time for PNT (b) degradation and (c) mineralization by SPEF process in actual wastewater.

Figure 3. Normalized PNT concentration decay over electrolysis time under optimized EF and SPEF conditions. The kinetic analysis of the concentration decays is presented in the inset panel.

Figure 4. Toxicity to *Artemia salina*, determined as a relationship between the number of dead individuals and the dilution employed.

Figure 5. Toxicity to *Lactuca sativa,* determined by germination index (GI%) for the treatment of effluents carried out under optimum EF and SPEF mineralization conditions.

Figure 6. Scheme showing three simultaneous PNT degradation routes occurring during the SPEF treatment.

a)

896
897

b)
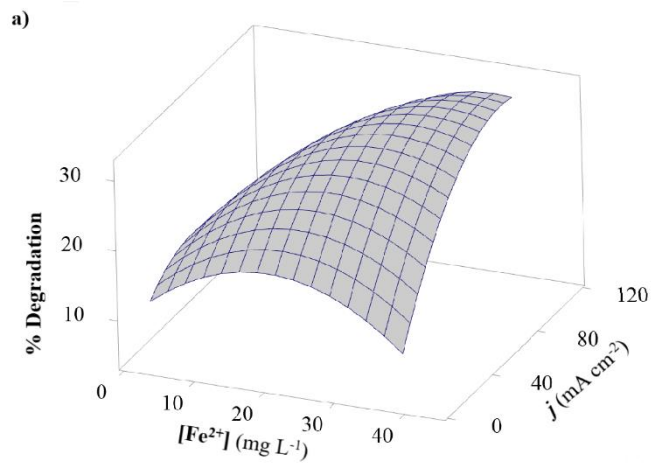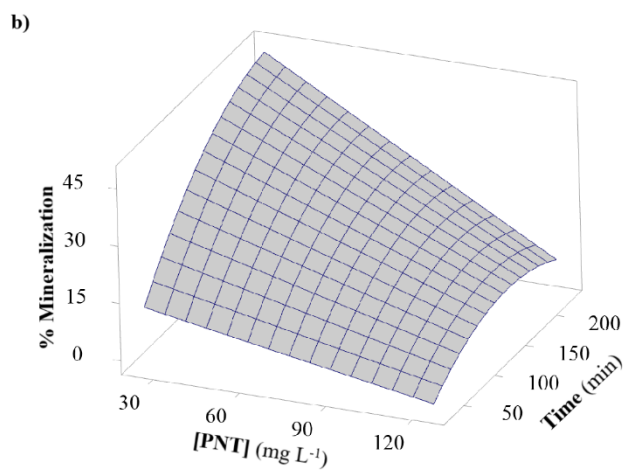
898
899
900
901
902
903

Figure 1

904

a)

905

906

b)

907

908

c)
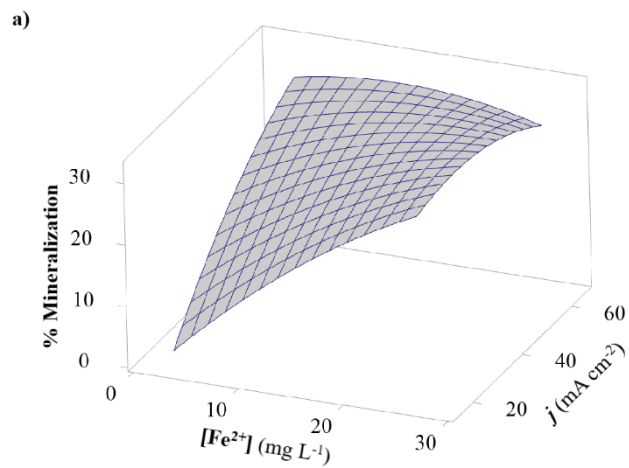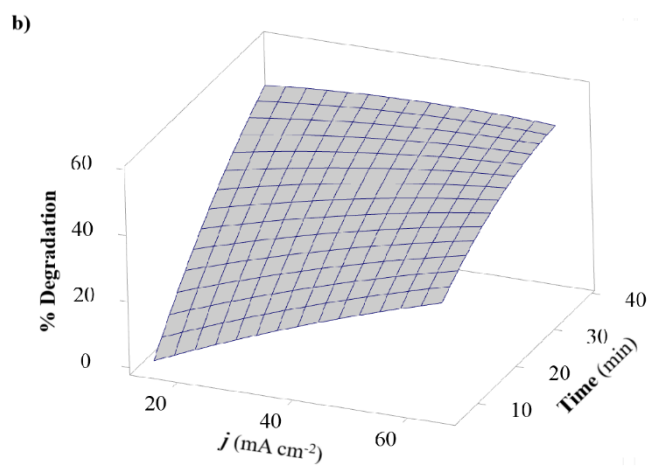
909

910
911   **Figure 2**

34

912
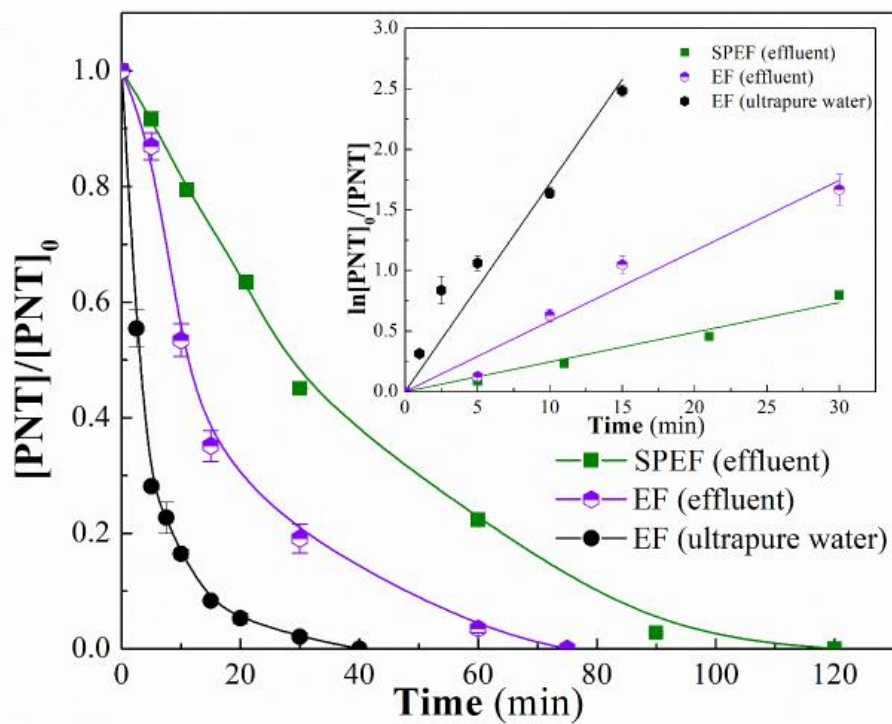
913
914
915
916
917
918

Figure 3
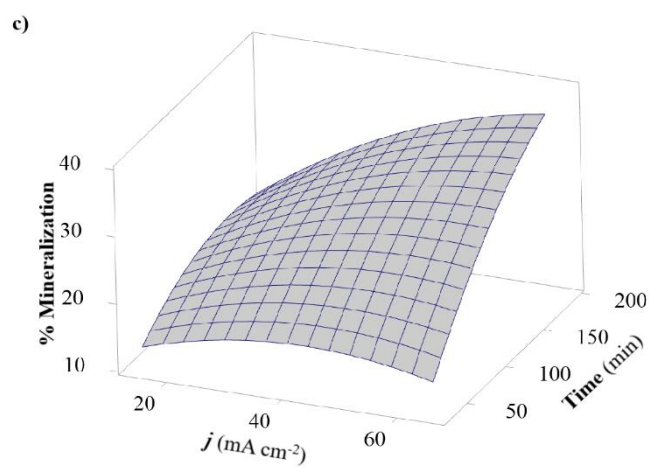
919

920

921

Figure 4

923
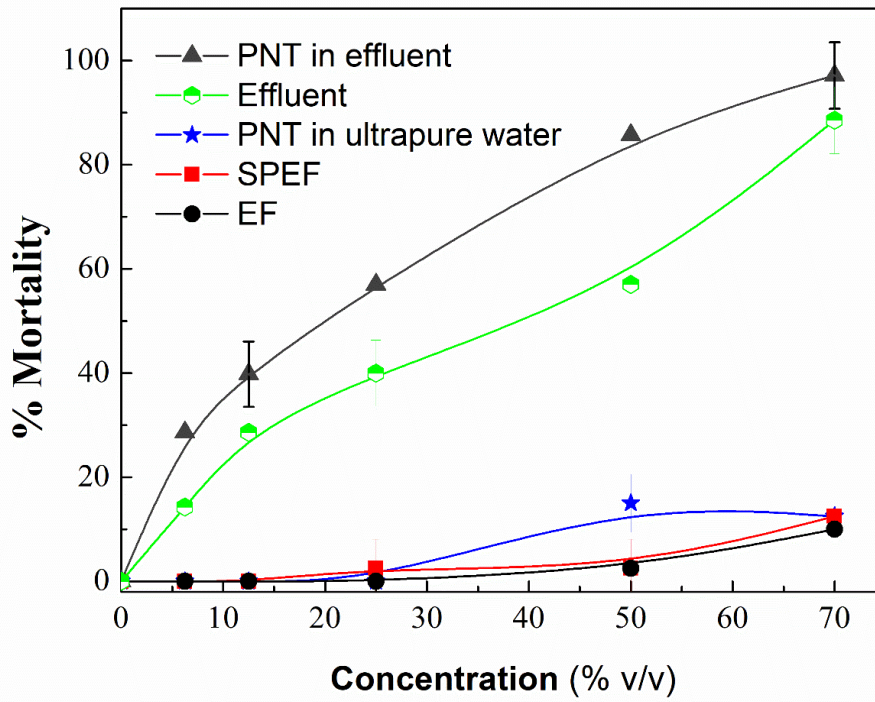
924
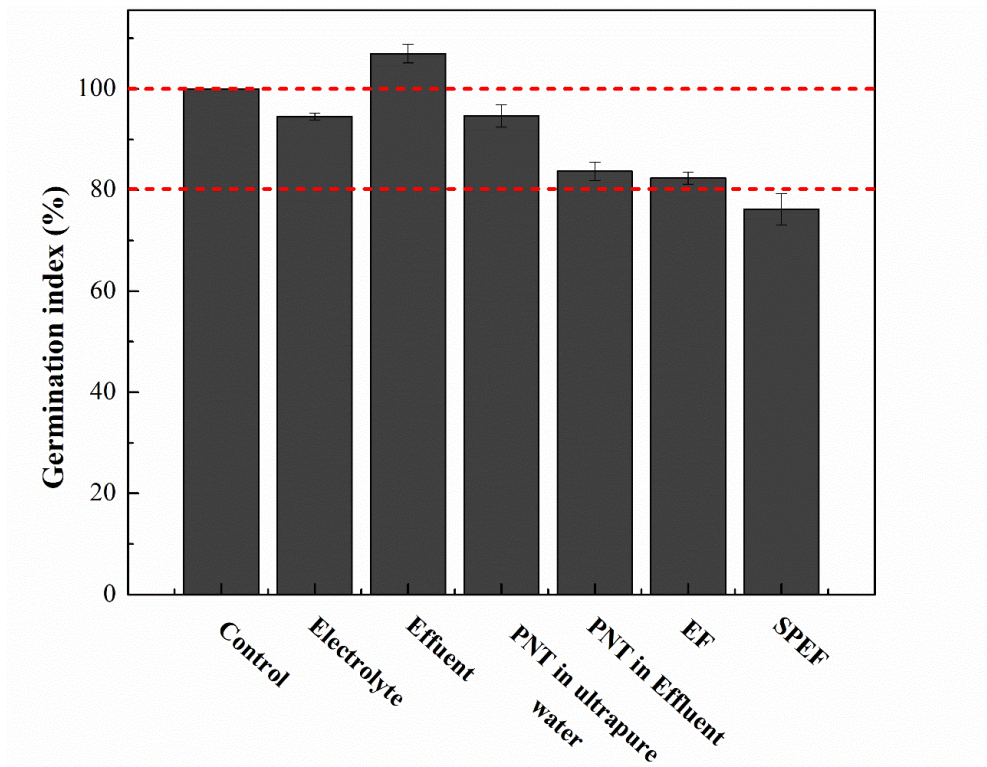
925

926

927

928 **Figure 5**
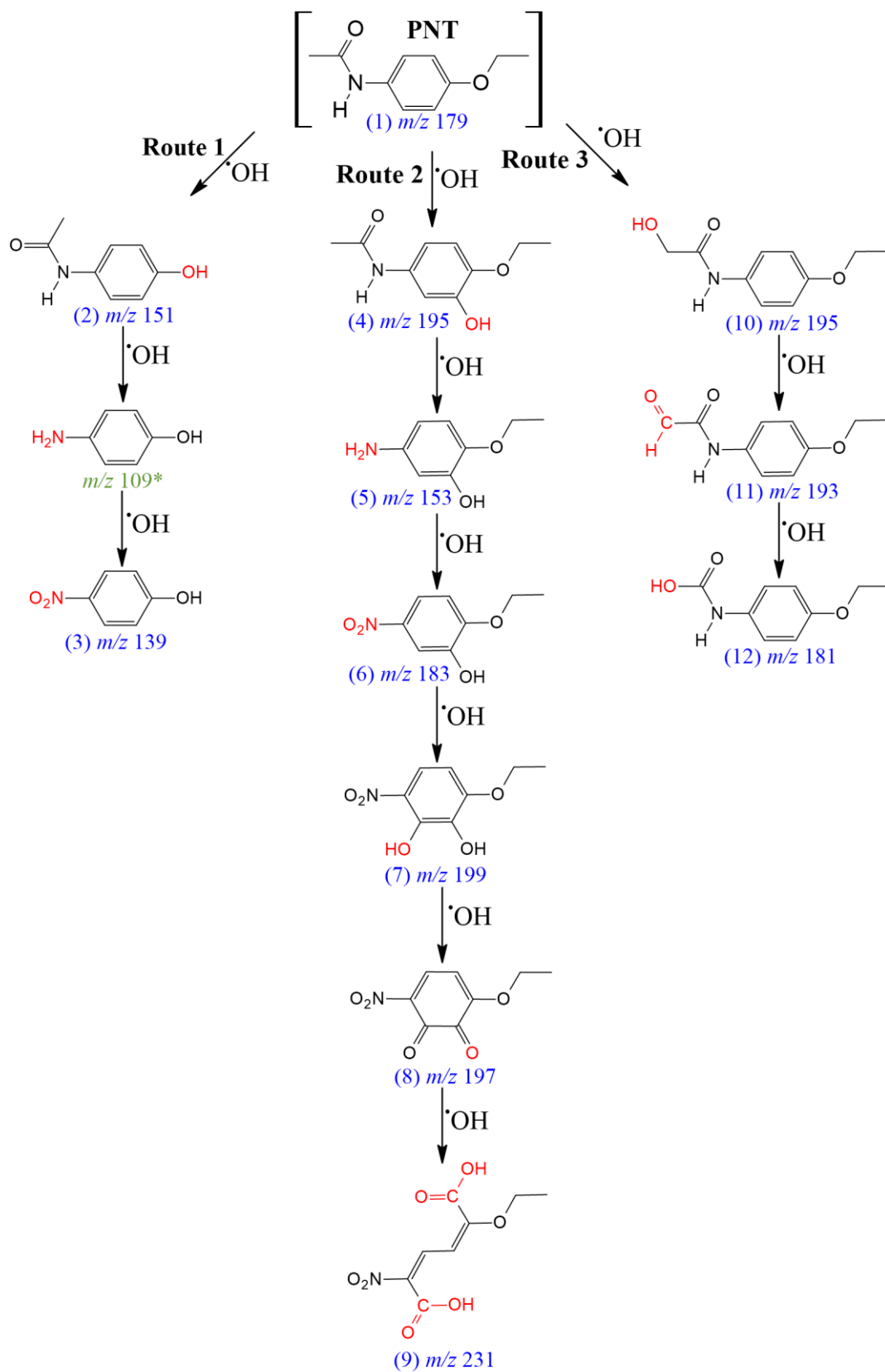
929

930

931 **Figure 6**

38

932　**Table 1.** Levels of the CCD 2^4 and CCD 2^3, indicating the values of the variables used to
933　investigate the PNT removal by EF and SPEF processes.[a]

EF process (laboratory scale)					
Variable[a]	**Level**				
	-2	-1	0	+1	+2
[PNT] / mg L^{-1}	25	50	75	100	125
[Fe^{2+}] / mg L^{-1}	1	15	29	43	57
j / mA cm^{-2}	10	35	60	85	110
Degradation time / min	2	5	8	11	14
Mineralization time / min	30	80	130	180	230
SPEF process (pre-pilot scale)					
Variable[a]	**Level**				
	-1.63	-1	0	+1	+1.63
[Fe^{2+}] / mg L^{-1}	3	8	15	22	27
j / mA cm^{-2}	15	25	40	55	65
Degradation time / min	6	12	21	30	36
Mineralization time / min	29	60	105	150	181

934　[a] The degradation and mineralization times were different and used separately to investigate the interactions.
935

Table 2. CCD 2^4 with the responses (Deg.: degradation; Min.: mineralization) obtained from the removal of PNT in a model solution by EF process.

Trial	[PNT] / mg L^{-1}	[Fe^{2+}] / mg L^{-1}	j / mA cm^{-2}	Time for Deg. / min	Time for Min. / min	Deg. Obs. (%)	Deg. Pred. (%)	Min. Obs. (%)	Min. Pred. (%)
1	75	29	60	8	130	27.2	28.0	22.8	23.4
2	75	29	60	14	230	45.0	42.2	25.9	26.3
3	75	1	60	8	130	16.0	14.5	9.8	12.1
4	**25**	**29**	**60**	**8**	**130**	**64.6**	**62.1**	**35.2**	**37.5**
5	75	29	60	2	30	11.3	14.2	5.9	5.5
6	75	29	110	8	130	26.5	24.9	11.0	9.1
7	125	29	60	8	130	20.8	23.4	11.7	9.4
8	75	29	60	8	130	29.2	28.0	23.8	23.4
9	75	29	10	8	130	16.0	17.7	12.5	14.3
10	75	57	60	8	130	25.0	26.6	29.0	26.6
11	75	29	60	8	130	29.2	28.4	26.8	24.5
12	100	15	35	5	80	8.7	8.2	5.3	5.1
13	100	43	85	5	80	24.0	21.0	9.0	10.6
14	50	15	85	5	80	27.2	29.0	12.8	15.4
15	100	43	85	11	180	30.5	33.1	16.0	19.0
16	50	15	85	11	180	40.0	41.9	32.9	30.3
17	75	29	60	8	130	28.4	28.4	24.0	24.5
18	100	15	35	11	180	20.8	20.7	9.7	10.3
19	100	43	35	11	180	28.9	26.1	24.6	21.7
20	50	43	35	5	80	29.8	28.2	24.6	23.0
21	50	43	85	5	80	34.6	35.7	18.8	18.6
22	100	15	85	5	80	12.0	10.9	3.5	1.8
23	100	43	35	5	80	12.0	11.1	12.7	15.7
24	75	29	60	8	130	27.2	28.4	23.9	24.5
25	75	29	60	8	130	28.6	28.4	23.5	24.5
26	50	43	85	11	180	51.8	51.2	34.3	34.2
27	100	15	85	11	180	19.9	20.4	8.2	9.5
28	50	43	35	11	180	44.5	46.6	34.1	36.2
29	50	15	35	5	80	30.3	28.7	20.6	18.0
30	50	15	35	11	180	42.7	44.6	32.4	30.4

940 **Table 3.** ANOVA results for PNT removal (Deg.: degradation; Min.: mineralization) by
941 EF process (see results from Table S2).

Source	Deg.			Min.		
	%	F-value	p-value	%	F-value	p-value
Model	98.0	45.0	0.000	96.2	23.9	0.000
Linear	81.8	141.0	0.000	81.0	75.4	0.000
[PNT]	49.3	340.2	0.000	43.8	163.0	0.000
$[Fe^{2+}]$	4.8	33.3	0.000	11.7	43.6	0.000
j	1.7	11.9	0.004	1.5	5.7	0.032
Time	25.9	178.6	0.000	24.0	89.6	0.000
Interaction	2.1	2.5	0.078	3.5	2.2	0.110
$[PNT]*[Fe^{2+}]$	0.3	1.7	0.209	1.2	4.4	0.055
[PNT]**j*	0.1	0.9	0.360	0.02	0.06	0.806
[PNT]*Time	0.3	1.8	0.203	2.0	7.2	0.018
$[Fe^{2+}]*j$	1.2	8.1	0.013	0.1	0.5	0.509
$[Fe^{2+}]*Time$	0.1	1.0	0.341	0.02	0.07	0.792
j*Time	0.2	1.3	0.273	0.2	0.8	0.383
Quadratic	14.0	24.2	0.000	11.5	10.7	0.000
[PNT]*[PNT]	10.5	56.4	0.000	0.5	0.0	0.982
$[Fe^{2+}]*[Fe^{2+}]$	1.8	14.7	0.002	0.2	3.8	0.072
j*j	1.8	11.9	0.004	7.3	32.1	0.000
Time*Time	0.04	0.01	0.938	3.6	13.3	0.002
Lack of fit	1.9	8.6	0.026	3.5	5.1	0.065
Error	2.0			3.8		
Summary	$R^2 = 98.0\%$; $R^2_{Adj} = 95.8\%$			$R^2 = 96.2\%$; $R^2_{Adj} = 92.2\%$		

942
943

944 **Table 4.** Results of PNT removal in real wastewater by EF and PEF under optimal
945 conditions.

Parameter	Process	EF	PEF	EC_{TOC} / kWh (g TOC)$^{-1}$
[PNT] = 25.0 mg L^{-1} [Fe^{2+}] = 25.3 mg L^{-1} j = 59.5 mA cm^{-2} Time for Deg. = 14 min Time for Min. = 230 min	Degradation	68.0% (±2.4)	89.5% (±1.0)	7.0
	Mineralization	39.4% (±1.3)	68.7% (±2.2)	

946
947

948 **Table 5.** CCD 2^3 with the responses (Deg.: degradation; Min.: mineralization) obtained
949 for the removal of PNT in real wastewater by SPEF process.

Trial	Factors				Deg.		Min.	
	$[Fe^{2+}]$ /mg L^{-1}	j /mA cm^{-2}	Time for Deg. / min	Time for Min. / min	Obs. (%)	Pred. (%)	Obs. (%)	Pred. (%)
1	3	40	21	105	27.4	27.5	16.9	18.1
2	8	55	12	60	30.2	28.4	21.5	20.2
3	**22**	**55**	**30**	**150**	**49.7**	**49.6**	**33.9**	**34.6**
4	8	25	30	150	39.9	41.4	17.0	17.3
5	22	55	12	60	37.0	35.8	22.6	22.3
6	15	40	21	105	38.3	39.8	26.5	27.2
7	15	40	6	29	16.5	18.0	15.8	16.9
8	15	65	21	105	44.2	46.2	28.3	29.0
9	15	15	21	105	32.4	30.0	19.9	19.1
10	22	25	30	150	42.9	45.0	29.7	31.0
11	8	55	30	150	45.6	45.5	31.9	31.5
12	15	40	21	105	40.9	39.8	28.0	27.2
13	27	40	21	105	37.3	36.7	32.6	31.3
14	8	25	12	60	13.3	13.7	12.8	12.1
15	22	25	12	60	20.4	20.7	24.2	24.6
16	**15**	**40**	**36**	**181**	**54.8**	**52.9**	**32.8**	**31.7**
17	15	40	21	105	40.0	39.8	27.1	27.2

950
951

Table 6. ANOVA results for PNT removal (Deg.: degradation; Min.: mineralization) by

953 SPEF process (see results from Table S4).

Source	Deg.			Min.		
	(%)	F-value	p-value	(%)	F-value	p-value
Model	98.5	51.2	0.000	98.2	42.1	0.000
Linear	91.3	142.3	0.000	84.6	108.8	0.000
$[Fe^{2+}]$	5.0	23.4	0.002	30.0	115.8	0.002
j	15.3	71.7	0.000	17.0	65.6	0.000
Time	70.9	331.6	0.000	37.6	145.1	0.000
Interaction	3.0	4.6	0.044	10.5	13.5	0.003
$[Fe^{2+}]*j$	0	0	0.897	7.9	30.2	0.001
$[Fe^{2+}]*$Time	0.3	1.3	0.291	0	0.3	0.582
$j*$Time	2.7	12.5	0.010	2.6	9.9	0.016
Quadratic	4.3	6.7	0.018	3.1	4.0	0.061
$[Fe^{2+}]*[Fe^{2+}]$	3.1	18.4	0.004	0.3	4.7	0.067
$j*j$	0	0.8	0.391	1.1	7.5	0.029
Time*Time	1.2	5.8	0.047	1.7	6.6	0.037
Lack of fit	1.3		0.258	1.7	4.1	0.209
Error	1.5					
Summary	$R^2 = 98.5\%$; $R^2_{Adj.} = 96.6\%$			$R^2 = 98.2\%$; $R^2_{Adj.} = 96.0\%$		

954

955

956   **Table 7.** Results of PNT removal in real wastewater by SPEF under optimal conditions.

Parameter	Process	Predicted	Observed	EC_{TOC} / kWh (g TOC)$^{-1}$
$[Fe^{2+}]$ = 16.8 mg L^{-1} j = 45.9 mA cm^{-2}	Degradation	53.2%	55.9% (±1.7)	
Time for Deg. = 36 min Time for Min. = 181 min $[Fe^{2+}]$ = 16.8 mg L^{-1}	Mineralization	34.5%	37.1% (±1.4)	0.142

957

958 **Table 8.** Comparison of the removal of PNT by other oxidative processes.

Process	PNT concentration / mM	Solution volume / L	Degradation	Ref.
O_3	20.0	0.1	95.0% in 30 min	[15]
UV/persulfate	0.025	0.1	96.3% in 30 min	[24]
Heterogeneous Fenton	0.010	0.25	76.0% in 60 min	[68]
MoS_2-assisted Fe^{2+}/PMS	0.025	0.25	94.3% in 15 min	[69]
UV/Cl_2	0.010	0.1	95.7% in 20 min	[70]
EF	0.139	0.1	83.9% in 14 min	Present study
SPEF	0.139	8	53.2% in 36 min	Present study

959

960

961

962